

# Rotation of a spheroid in a simple shear at small Reynolds number

J. Einarsson,<sup>1</sup> F. Candelier,<sup>2</sup> F. Lundell,<sup>3</sup> J. R. Angilella,<sup>4</sup> and B. Mehlig<sup>1</sup>

<sup>1</sup>*Department of Physics, Gothenburg University, 41296 Gothenburg, Sweden*

<sup>2</sup>*University of Aix-Marseille, CNRS, IUSTI UMR 7343, 13 013 Marseille, Cedex 13, France*

<sup>3</sup>*KTH Royal Institute of Technology, SE-100 44 Stockholm, Sweden*

<sup>4</sup>*Department of Mathematics and Mechanics, LUSAC-ESIX, University of Caen, France*

We derive an effective equation of motion for the orientational dynamics of a neutrally buoyant spheroid suspended in a simple shear flow, valid for arbitrary particle aspect ratios and to linear order in the shear Reynolds number. We show how inertial effects lift the degeneracy of the Jeffery orbits and determine the stabilities of the log-rolling and tumbling orbits at infinitesimal shear Reynolds numbers. For prolate spheroids we find stable tumbling in the shear plane, log-rolling is unstable. For oblate particles, by contrast, log-rolling is stable and tumbling is unstable provided that the aspect ratio is larger than a critical value. When the aspect ratio is smaller than this value tumbling turns stable, and an unstable limit cycle is born.

PACS numbers: 83.10.Pp, 47.15.G-, 47.55.Kf, 47.10.-g

## I. INTRODUCTION

In this article we describe the effect of weak inertia upon the orientational dynamics of a neutrally buoyant spheroid in a simple shear flow using perturbation theory. In the absence of inertial effects the rotation of a neutrally buoyant spheroid in a simple shear was determined by Jeffery who found that there are infinitely many degenerate periodic orbits<sup>1</sup>, the so-called ‘Jeffery orbits’. In this limit the initial orientation determines in which way the particle rotates. Fluid and particle inertia lift this degeneracy, but little is known about how this comes about. A notable exception is the work by Subramanian and Koch who have solved the problem for rod-shaped particles in the slender-body approximation<sup>2</sup>. We discuss other theoretical results below in Section II.

The question is currently of great interest: several recent papers have reported results of direct numerical simulations (DNS) of the problem, using ‘lattice Boltzmann’ methods<sup>3–6</sup>. These studies reveal that fluid and particle inertia affect the orientational dynamics of a neutrally buoyant spheroid in a simple shear in intricate ways. The DNS are performed at moderate and large shear Reynolds numbers, defined as  $Re_s = sa^2/\nu$  where  $a$  is the largest particle dimension,  $s$  is the shear strength and  $\nu$  the kinematic viscosity of the suspending fluid. DNS at very small Reynolds numbers are difficult to perform. But this limit ( $Re_s$  of order unity and smaller) is of particular interest. There is a long-standing question whether or not a nearly spherical prolate spheroid exhibits stable ‘log-rolling’ in this limit, so that its symmetry axis aligns with the vorticity axis. It was first suggested by Saffman that this is the case<sup>7</sup>, in an attempt to explain Jeffery’s hypothesis<sup>1</sup> that spheroids rotate in orbits that minimise energy dissipation. But stable log-rolling of prolate spheroids has not been found in DNS, and it has been suggested that higher  $Re_s$ -corrections may explain this discrepancy<sup>6</sup>. The small- $Re_s$  limit is of interest also because it provides stringent tests for DNS. These reasons motivated us to derive an equation of motion that takes into account the effect of weak fluid and particle inertia. Our main result is an approximate dynamical equation for the rotation of a neutrally buoyant spheroid suspended in a simple shear flow, valid for arbitrary aspect ratios and to first order in  $Re_s$  (Eq. (42) in Section IV). In the slender-body limit this equation is of the same form as the one derived in Ref. 2. In the completely inertia-free case our results reduce to Jeffery’s equation<sup>1</sup>. We find that corrections to this limit arise from both particle inertia (centrifugal and gyroscopic forces), as well as from fluid inertia (modifying the hydrodynamic torque on the particle). The particle-inertia corrections we report here are consistent with earlier numerical and analytical results<sup>8,9</sup>.

Fluid-inertia corrections are taken into account to first order in  $Re_s$  using a reciprocal theorem<sup>10</sup>. Our approach is similar to the one adopted in Ref. 2 in the slender-body limit, but our equation of motion is valid for spheroids with arbitrary aspect ratios. By linear stability analysis we determine the stabilities of the periodic orbits of this equation at infinitesimal  $Re_s$  as a function of the particle aspect ratio. The stability calculation details how the degeneracy of the Jeffery orbits for a neutrally buoyant spheroid in a simple shear is lifted by weak inertia.

We find that the log-rolling orbit is unstable for prolate particles. This explains why stable log-rolling is

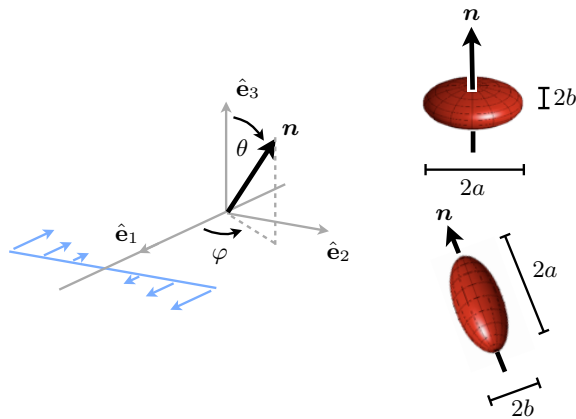


FIG. 1. *Color online.* Spheroid rotating in a simple shear (schematic). Shows the Cartesian coordinate system  $\hat{e}_j$ ,  $j = 1, \dots, 3$ . Vorticity points in the negative  $\hat{e}_3$ -direction. The flow-shear plane is spanned by  $\hat{e}_1$  and  $\hat{e}_2$ . The unit vector  $\mathbf{n}$  points along the symmetry axis of the spheroid. Its polar angle is denoted by  $\theta$ , the azimuthal angle by  $\varphi$ . The major axis length of the spheroid is denoted by  $a$ , the minor length by  $b$ . For prolate particles the aspect ratio is defined as  $\lambda = a/b$ , and for oblate particles as  $\lambda = b/a$ .

not observed in DNS<sup>3-6</sup> at the smallest shear Reynolds numbers accessible in the simulations. Moreover we find that tumbling in the flow-shear plane is stable for prolate particles. As the aspect ratio tends to unity there is a bifurcation: for nearly spherical oblate particles log-rolling is stable and tumbling in the flow-shear plane is unstable. There is a second bifurcation for oblate particles. At a critical aspect ratio  $\lambda_c \approx 1/7.3$  tumbling becomes stable and an unstable limit cycle is born. This means that the behaviour of a very flat disk depends on its initial orientation for  $\lambda < \lambda_c$ . We discuss how the shape of the limit cycle changes as the aspect ratio tends to zero.

The remainder of this article is organised as follows. In Section II we give an overview over the background of the problem. Section III summarises the method employed in this article, based on a reciprocal theorem<sup>10</sup>. We demonstrate how to calculate the effect of particle and fluid inertia to first order, and how we use the symmetries of the problem to make it tractable. Section IV summarises our results: the equation of motion and its stability analysis. We discuss the results in Section V and conclude with Section VI.

A brief account of the main results described in this article was given in Ref. 11. Here we describe the complete derivation. We also present additional results and discussion that could not be included in the shorter format: we quote precise asymptotic formulae for small and large aspect ratios, as well as for aspect ratios close to unity. We also characterise the limit cycle that arises for  $\lambda < \lambda_c$ , and compute its linear stability.

## II. BACKGROUND

The question of describing the rotation of a neutrally buoyant particle in a simple shear flow has a long history. Jeffery derived an expression for the torque on an ellipsoidal (tri-axial) particle neglecting inertial effects<sup>1</sup>. To obtain an equation of motion for small particles he assumed that the dynamics is overdamped, that the particle rotates so as to instantaneously achieve zero torque. This gives rise to Jeffery's equation that is commonly quoted for the special case of spheroidal (axisymmetric) particles. From this equation it follows that spheroids suspended in a simple shear tumble, they stay aligned with the flow direction for some time and then switch orientation by 180 degrees. The dynamics is degenerate in that there are infinitely many different periodic orbits, the so-called 'Jeffery orbits'. The initial orientation determines which particular orbit is selected. The goal of Jeffery's calculation was to compute the viscosity of a dilute suspension of spheroids, and Jeffery hypothesised that the particles select orbits that minimise energy dissipation.

Saffman<sup>7</sup> pointed out that inertial effects lift the degeneracy of the Jeffery orbits, and he described the orientational dynamics of a nearly spherical particle in a simple shear taking into account fluid inertia. For prolate particles he concluded that log-rolling is stable, that tumbling in the shear plane is unstable, and that the stabilities are reversed for oblate particles. These results are stated in terms of an effective drift for

the particle orientation (towards the vorticity axis for prolate particles). This conclusion supports Jeffery's hypothesis. Saffman did not take into account particle inertia. His method of calculation rests on a joint expansion in small eccentricity and  $Re_s$ .

Harper & Chang<sup>12</sup> addressed the problem in a different way, modeling the dynamics of a rod in a simple shear in terms a dumb-bell, that is two spheres connected by an invisible rigid rod. The spheres are subject to Stokes drag and hydrodynamic lift forces<sup>13</sup>. This approximation neglects hydrodynamic interactions between the two spheres, as well as the unsteady term in the Navier-Stokes equations. Harper & Chang arrive at the opposite conclusion, namely that log-rolling is unstable. Since their result pertains to the slender-body limit the question is how the stability of the log-rolling orbit depends on the particle aspect ratio.

It was subsequently shown by Hinch & Leal<sup>14</sup> how weak rotational diffusion breaks the degeneracy of the Jeffery orbits, and their results form the basis for a large part of the work during the last decades on the rheology of dilute suspensions, see Refs. 15 and 16 for reviews.

Recently there has been a surge of interest in determining the effect of weak inertia upon a spheroid tumbling in a simple shear flow in the absence of rotational diffusion. Subramanian & Koch<sup>2</sup> derived an effective equation of motion for a neutrally buoyant rod in the slender-body limit to first order in fluid and particle inertia. Their calculation uses a reciprocal theorem<sup>10</sup> and takes into account the unsteady term in the Navier Stokes equation as well as particle inertia. The authors arrive at qualitatively the same conclusion as Harper & Chang, namely that the orientation of the rod eventually drifts towards the flow-shear plane.

In a second paper Subramanian & Koch<sup>17</sup> repeated Saffman's calculation for a neutrally buoyant nearly spherical particle. They used a different method, similar to the one used in Ref. 2, and come to the same conclusion as Saffman, that log-rolling is stable for nearly-spherical prolate particles.

Recent DNS<sup>3-6</sup> have explored the stability of log-rolling and tumbling orbits, mostly at moderate and large Reynolds numbers, and only for a small number of aspect ratios. The simulations show unstable log-rolling for prolate particles at the smallest Reynolds numbers studied. We note that You, Phan-Thien & Tanner<sup>18</sup> misquote Saffman when they describe their numerical results on the rotation of a spheroid in a Couette flow at Reynolds numbers of the order of 10 and larger. In the introduction of Ref. 18 it is implied that Saffman's theory<sup>7</sup> predicts that nearly spherical prolate particles tend to the flow-shear plane.

### III. METHOD

In this section we give a brief but complete summary of our calculation. The most technical details and tabulations are deferred to appendices. We start with notation and the relevant dimensionless parameters determining the physics. Then we give the governing equations and explain how to express the hydrodynamic torque through a reciprocal theorem<sup>2,10,19,20</sup>. Finally we explain the perturbation scheme and list the symmetries that severely constrain the form of the solution.

#### A. Notation

The calculations described in this paper involve vectors and tensors in three spatial dimensions. We employ index notation with the implicit summation convention for repeated indices, and we use the Kronecker ( $\delta_{ij}$ ) and Levi-Civita ( $\varepsilon_{ijk}$ ) tensors.

#### B. Units and dimensionless numbers

The physics of the problem is governed by three dimensionless numbers: the shear Reynolds number  $Re_s$  (measuring fluid inertia), the Stokes number  $St$  (measuring particle inertia) and the particle aspect ratio  $\lambda$ .

We work with dimensionless variables. The length scale is given by the particle major axis  $a$ . The velocity scale is taken to be  $sa$  where  $s$  is the shear rate. The explicit time dependence of the flow (the time scale for the unsteady fluid inertia) scales as  $\sim 1/s$  since it is determined by the particle angular velocity because to lowest order the unsteadiness arises from the particle motion. The corresponding scale for pressure is  $\mu s$ , and force and torque are measured in units of  $\mu sa^2$  and  $\mu sa^3$ , respectively.

From these scales the dimensionless parameters are formed. As mentioned in the Introduction, the shear Reynolds number is defined as

$$\text{Re}_s = \frac{sa^2\rho_f}{\mu}. \quad (1)$$

Here  $\rho_f$  is the density and  $\mu = \rho_f\nu$  is the dynamic viscosity of the surrounding fluid ( $\nu$  is the kinematic viscosity).

The Stokes number, measuring the particle inertia, is given by the ratio of the typical rate of change of angular momentum and the typical torque:

$$\text{St} = \frac{\rho_p sa^2}{\mu} = \frac{\rho_p}{\rho_f} \text{Re}_s. \quad (2)$$

Here  $\rho_p$  is the particle density. For a neutrally buoyant particle,  $\rho_p = \rho_f$ , we have  $\text{St} = \text{Re}_s$ .

We define the particle aspect ratio  $\lambda$  as the ratio between the length along the symmetry axis and the length transverse to the symmetry axis (Fig. 1). That is  $\lambda > 1$  denotes prolate particles while  $\lambda < 1$  denotes oblate particles. Because we measure length in units of the major particle axis  $a$ , the aspect ratio  $\lambda$  of a prolate particle is  $a/b$ , while the aspect ratio of an oblate particle is  $b/a$ , where  $b$  denotes the length of the minor axis of the particle (see Fig. 1).

### C. Equations of motion

Let  $n_i$  denote the components of the unit vector  $\mathbf{n}$  pointing in the direction of the particle symmetry axis (Fig. 1), and  $\omega_i$  the components of the angular velocity of the particle. Newton's second law for the orientational degrees of freedom for an axisymmetric particle reads:

$$\dot{n}_i = \varepsilon_{ijk}\omega_j n_k, \quad \text{St} \left[ \dot{I}_{ij}\omega_j + I_{ij}\dot{\omega}_j \right] = T_i. \quad (3)$$

Dots denote time derivatives, and  $I_{ij}$  are the elements of the moment-of-inertia tensor of the particle, and  $T_i$  is the torque exerted on the particle. The moment-of-inertia tensor of an axisymmetric particle with axis of symmetry  $\mathbf{n}$  is on the form

$$I_{ij} = A^I n_i n_j + B^I (\delta_{ij} - n_i n_j), \quad (4)$$

where  $A^I$  and  $B^I$  correspond to the moments-of-inertia around and transverse to the symmetry axis. Using the dimensionless variables introduced in Section III B we have for a prolate spheroid ( $\lambda > 1$ )

$$A^I = \frac{8\pi}{15} \frac{1}{\lambda^4}, \quad B^I = \frac{4\pi}{15} \frac{1}{\lambda^2} \left( 1 + \frac{1}{\lambda^2} \right) \quad (5)$$

and for an oblate spheroid ( $\lambda < 1$ )

$$A^I = \frac{8\pi}{15} \lambda, \quad B^I = \frac{4\pi}{15} \lambda (1 + \lambda^2). \quad (6)$$

We rewrite the equation of motion (3) as

$$\dot{\omega}_i = -I_{ij}^{-1} \dot{I}_{jk} \omega_k + \frac{1}{\text{St}} I_{ij}^{-1} T_j = -\frac{A^I - B^I}{B^I} \varepsilon_{ijk} \omega_j n_k n_l \omega_l + \frac{1}{\text{St}} I_{ij}^{-1} T_j. \quad (7)$$

In the final step we used the definition (4) of  $I_{ij}$  and the equation of motion (3) for  $\dot{n}_i$ .

In this paper, the  $T_i$  are the elements of the hydrodynamic torque exerted on the particle by the fluid. In Section III D we formulate the hydrodynamic torque to  $O(\text{Re}_s)$  via the reciprocal theorem. In Section III E we perturbatively compute the resulting angular velocity to order  $O(\text{Re}_s)$  and  $O(\text{St})$ .

#### D. Calculation of the hydrodynamic torque to order $\text{Re}_s$

The straightforward approach to determine the torque on a particle in a fluid is to solve Navier-Stokes equations for the velocity and pressure fields, then compute the stress tensor and finally integrate the stress tensor over the surface of the particle. The reciprocal theorem<sup>2,10,19</sup> offers an alternative, and often more convenient, route to the hydrodynamic forces. In particular, we may avoid solving for the complete flow field. In this Section we specify the Navier-Stokes problem we need to solve, and explain how we use the reciprocal theorem to simplify the calculations.

*Navier-Stokes problem for the disturbance flow.* We consider a particle with boundary  $\mathcal{S}$  immersed in an linear ambient flow  $(\mathbf{u}^\infty, p^\infty)$ . Throughout this paper we express the ambient flow as

$$u_i^\infty = A_{ij}^\infty r_j = \varepsilon_{ikj} \Omega_k^\infty r_j + S_{ij}^\infty r_j, \quad (8)$$

or equivalently with  $\varepsilon_{ikj} \Omega_k^\infty = O_{ij}^\infty$

$$u_i^\infty = O_{ij}^\infty r_j + S_{ij}^\infty r_j. \quad (9)$$

Here  $\mathbf{S}^\infty$  and  $\mathbf{O}^\infty$  are the symmetric and antisymmetric parts of the flow gradient, given by

$$S_{ij}^\infty = \frac{1}{2} (A_{ij}^\infty + A_{ji}^\infty), \quad O_{ij}^\infty = \frac{1}{2} (A_{ij}^\infty - A_{ji}^\infty). \quad (10)$$

In dimensionless variables (Section III B) the Navier-Stokes equations read

$$\text{Re}_s (\partial_t u_i + u_j \partial_j u_i) = -\partial_i p + \partial_j \partial_j u_i, \quad \partial_i u_i = 0. \quad (11)$$

Note that the unsteady and convective inertia terms come with the same prefactor in this problem. This happens because the timescale of the particle motion is the same as the timescale of the flow. The boundary condition is no-slip on the surface of the particle

$$u_i = \varepsilon_{ijk} \omega_j r_k \text{ for } \mathbf{r} \in \mathcal{S}, \quad u_i = u_i^\infty \text{ as } |\mathbf{r}| \rightarrow \infty. \quad (12)$$

We introduce the disturbance field  $(u'_i, p')$  from the particle

$$u_i = u_i^\infty + u'_i, \quad p = p^\infty + p'. \quad (13)$$

If we assume that  $(\mathbf{u}^\infty, p^\infty)$  satisfies the Navier-Stokes equations we have the disturbance problem

$$\text{Re}_s (\partial_t u'_i + u_j^\infty \partial_j u'_i + u'_j \partial_j u_i^\infty + u'_j \partial_j u'_i) = -\partial_i p' + \partial_j \partial_j u'_i, \quad (14)$$

and the boundary conditions is expressed in the slip angular velocity  $\Omega_i = \Omega_i^\infty - \omega_i$  as

$$\begin{aligned} u'_i &= -\varepsilon_{ijk} \Omega_j r_k - S_{ij}^\infty r_j, \quad \mathbf{r} \in \mathcal{S}, \\ u'_i &= 0, \quad |\mathbf{r}| \rightarrow \infty. \end{aligned} \quad (15)$$

Finally, when applying the reciprocal theorem we shall use that, by definition, the divergence of the stress tensor satisfies the following equalities:

$$\begin{aligned} \partial_j \sigma'_{ij} &= -\partial_i p' + \partial_j \partial_j u'_i \\ &= \text{Re}_s (\partial_t u'_i + u_j^\infty \partial_j u'_i + u'_j \partial_j u_i^\infty + u'_j \partial_j u'_i) \\ &\equiv \text{Re}_s f_i(\mathbf{u}'). \end{aligned} \quad (16)$$

*The Stokes solution.* This paper concerns a spheroidal particle suspended in a linear flow. We thus need explicit solutions to Eq. (14) at  $\text{Re}_s = 0$  in this geometry. We use a finite multipole expansion<sup>10,21</sup> (see Appendix A). In our notation they read

$$\begin{aligned} u'_i &= \mathcal{Q}_{ij,k}^R \varepsilon_{jkl} [(A^R n_l n_m + B^R (\delta_{lm} - n_l n_m)) \Omega_m + C^R \varepsilon_{lmn} n_m S_{no}^\infty n_o] \\ &\quad + (\mathcal{Q}_{ij,k}^S + \alpha \mathcal{Q}_{ij,llk}^Q) \\ &\quad \times [(A^S n_{jklm}^A + B^S n_{jklm}^B + C^S n_{jklm}^C) S_{lm}^\infty - C^R (\varepsilon_{jlm} n_k n_m + \varepsilon_{klm} n_j n_m) \Omega_l], \end{aligned} \quad (17)$$

where

$$\begin{aligned}
n_{jklm}^A &= (n_j n_k - \frac{1}{3} \delta_{jk})(n_l n_m - \frac{1}{3} \delta_{lm}), \\
n_{jklm}^B &= n_j \delta_{kl} n_m + n_k \delta_{jl} n_m + n_j \delta_{km} n_l + n_k \delta_{jm} n_l - 4n_j n_k n_l n_m, \\
n_{jklm}^C &= -\delta_{jk} \delta_{lm} + \delta_{jl} \delta_{km} + \delta_{kl} \delta_{jm} \\
&\quad + \delta_{jk} n_l n_m + \delta_{lm} n_j n_k - n_j \delta_{kl} n_m - n_k \delta_{jl} n_m \\
&\quad - n_j \delta_{km} n_l - n_k \delta_{jm} n_l + n_j n_k n_l n_m.
\end{aligned}$$

Here  $A^R, B^R, C^R, A^S, B^S, C^S$  and  $\alpha$  are known constants that depend on the particle aspect ratio  $\lambda$ . The exact definition of the spheroidal multipoles  $\mathcal{Q}$  and the values of all constants are given in Appendix A, see in particular Table III.

*The reciprocal theorem.* This theorem<sup>2,10,19,20</sup> relates integrals of the velocity and stress fields of two incompressible and Newtonian fluids. The idea is the following. Let one set of fields represent the actual problem of interest, the *primary problem*. Then choose the second set of fields to be an *auxiliary problem* with known solution, such that an integral in the theorem relates to hydrodynamic torque of the primary problem. Provided that all integrals in the theorem converge and can be evaluated, we can solve the resulting equations for the hydrodynamic torque.

The reciprocal theorem for the two sets  $(\tilde{u}_i, \tilde{\sigma}_{ij})$  and  $(u'_i, \sigma'_{ij})$  can be stated as

$$\int_S d\tilde{F}_i u'_i + \int_V dV u'_i \partial_j \tilde{\sigma}_{ij} = \int_S dF'_i \tilde{u}_i + \int_V dV \tilde{u}_i \partial_j \sigma'_{ij}. \quad (18)$$

Here  $dF_i = \sigma_{ij} \xi_j dS$  is the differential force from the fluid on the surface element with normal vector  $\xi_j dS$ . The volume integrals are to be taken over the entire fluid volume outside the particle, and the surface integrals over all surfaces bounding the fluid volume, with surface normals pointing out of the fluid volume.

In the following we apply the reciprocal theorem to the calculation of the hydrodynamic torque on a particle.

*Calculation of the torque.* We choose the auxiliary problem  $(\tilde{u}_i, \tilde{\sigma}_{ij})$  to be the Stokes flow around an identical particle rotating with an angular velocity  $\tilde{\omega}_i$  in an otherwise quiescent fluid. Its solution is given by Eq. (17) with  $\mathbf{u}^\infty = 0$ . The primary problem is the disturbance problem defined in Eq. (14). Inserting the boundary conditions into the reciprocal theorem yields

$$\int_S d\tilde{F}_i (\varepsilon_{ijk} (\omega_j - \Omega_j^\infty) r_k - S_{ij}^\infty r_j) = \int_S dF'_i \varepsilon_{ijk} \tilde{\omega}_j r_k + \text{Re}_s \int_V dV \tilde{u}_i f_i(\mathbf{u}'). \quad (19)$$

We also used that  $\partial_j \tilde{\sigma}_{ij} = 0$ . This equality holds because  $\tilde{u}_i$  is a Stokes flow. Both primary and auxiliary velocity fields vanish as  $|\mathbf{r}| \rightarrow \infty$ , therefore both integration surfaces are only the particle surface  $\mathcal{S}$ . Note that the surface integrals are to be taken with surface normals out of the fluid domain, so that  $dF'_i$  is the differential force exerted on the particle by the fluid. In the integrals we identify the hydrodynamic torque on the particle, it is given by

$$T_j = \int_S dF_i \varepsilon_{ijk} r_k. \quad (20)$$

It follows:

$$(\omega_j - \Omega_j^\infty) \tilde{T}_j - \int_S d\tilde{F}_i S_{ij}^\infty r_j = \tilde{\omega}_j (T_j - T_j^\infty) + \text{Re}_s \int_V dV \tilde{u}_i f_i(\mathbf{u}'). \quad (21)$$

The auxiliary torque  $\tilde{T}_j$  together with the surface integral add up to the Jeffery torque<sup>1</sup>  $T_j^{(0)}$ :

$$T_j^{(0)} = c_\xi [(A^R n_j n_k + B^R (\delta_{jk} - n_j n_k)) (\Omega_k^\infty - \omega_k) + C^R \varepsilon_{jkm} n_k n_l S_{ml}^\infty]. \quad (22)$$

The constant  $c_\xi$  is given in Table III in Appendix A. The contribution

$$T_j^\infty \equiv \int_S dS \sigma_{il}^\infty \xi_l \varepsilon_{ijk} \tilde{\omega}_j r_k \quad (23)$$

evaluates to zero for any linear flow  $u_i^\infty$ . It follows that Eq. (21) becomes

$$\tilde{\omega}_j T_j = \tilde{\omega}_j T_j^{(0)} - \text{Re}_s \int_V dV \tilde{u}_i f_i(\mathbf{u}'). \quad (24)$$

Since  $\tilde{u}_i$  is linear in  $\tilde{\omega}_j$ , this variable can be eliminated. We finally obtain:

$$T_j = T_j^{(0)} - \text{Re}_s \int_V dV \tilde{U}_{ij} f_i(\mathbf{u}'), \quad (25)$$

where

$$\begin{aligned} \tilde{U}_{ip} = & -\mathcal{Q}_{ij,k}^R \varepsilon_{jkl} [(A^R n_l n_p + B^R (\delta_{lp} - n_l n_p))] \\ & + \left( \mathcal{Q}_{ij,k}^S + \alpha \mathcal{Q}_{ij,llk}^Q \right) [C^R (\varepsilon_{jpm} n_k n_m + \varepsilon_{kpm} n_j n_m)]. \end{aligned} \quad (26)$$

Thus far we have made no approximation, and Eq. (25) is exact, the difficulty lies in evaluating the Navier-Stokes disturbance flow  $\mathbf{u}'$ . This is a complicated non-linear problem since  $T_j^{(0)}$ ,  $\tilde{U}_{ij}$  and  $f_i(\mathbf{u}')$  all depend on the direction  $\mathbf{n}$  and upon the angular velocity  $\boldsymbol{\omega}$  of the particle. The flow equations thus couple non-linearly to the rigid body equations of motion for the particle. In the following we solve this system of equations in perturbation theory valid to first order in  $\text{St}$  and  $\text{Re}_s$ .

### E. Perturbative calculation of the particle angular velocity

In this section we determine the angular velocity  $\boldsymbol{\omega}$  of the particle to lowest order in  $\text{St}$  and  $\text{Re}_s$ , assuming that both  $\text{St}$  and  $\text{Re}_s$  are small, so that  $\text{Re}_s \text{St}$  is negligible. We recall the equation of motion (7) for the particle orientation, and insert the expression for the hydrodynamic torque obtained in Section III D:

$$\begin{aligned} \dot{n}_i &= \varepsilon_{ijk} \omega_j n_k, \\ \text{St} \dot{\omega}_i &= -\text{St} \frac{A^I - B^I}{B^I} \varepsilon_{ijk} \omega_j n_k n_l \omega_l + I_{ij}^{-1} T_j^{(0)} - \text{Re}_s I_{ij}^{-1} \int_V dV \tilde{U}_{kj} f_k(\mathbf{u}'). \end{aligned} \quad (27)$$

Now we expand the angular velocity as

$$\omega_i = \omega_i^{(0)} + \text{St} \omega_i^{(\text{St})} + \text{Re}_s \omega_i^{(\text{Re}_s)} + o(\text{Re}_s, \text{St}). \quad (28)$$

Next, we insert these expansions into the equation of motion (7) and collect terms of equal order in  $\text{St}$  and  $\text{Re}_s$ :

$$\begin{aligned} 0 &= T_j^{(0)}, \\ \dot{\omega}_i^{(0)} &= -\frac{A^I - B^I}{B^I} \varepsilon_{ijk} \omega_j^{(0)} n_k n_l \omega_l^{(0)} - I_{ij}^{-1} c_\xi (A^R n_j n_k + B^R (\delta_{jk} - n_j n_k)) \omega_i^{(\text{St})}, \\ 0 &= c_\xi (A^R n_j n_k + B^R (\delta_{jk} - n_j n_k)) \omega_i^{(\text{Re}_s)} + \int_V dV \tilde{U}_{kj} f_k(\mathbf{u}'). \end{aligned} \quad (29)$$

In the last term it is understood that the volume integral need only be evaluated to  $O(1)$ , so that we may use the Stokes flow solutions for  $\mathbf{u}'$ . The first equation gives the Jeffery angular velocity  $\omega_i^{(0)}$ ,

$$\omega_i^{(0)} = \Omega_i^\infty + \frac{C^R}{B^R} \varepsilon_{ikm} n_k n_l S_{ml}^\infty. \quad (30)$$

The dynamics of  $\mathbf{n}$  is to lowest order given by

$$\dot{n}_i^{(0)} = \varepsilon_{ipq} \omega_p^{(0)} n_q \varepsilon_{ipq} \Omega_p^\infty n_q + \frac{C^R}{B^R} (S_{ip}^\infty n_p - n_i n_p n_q S_{pq}^\infty). \quad (31)$$

From Table III in Appendix A we infer that for both prolate and oblate spheroids

$$\frac{C^R}{B^R} = \Lambda = \frac{\lambda^2 - 1}{\lambda^2 + 1}. \quad (32)$$

This shows that Eq. (31) is Jeffery's equation<sup>1</sup> for the orientational dynamics of a spheroid in a simple shear. The two remaining equations in (29) may be inverted to

$$\begin{aligned}\omega_i^{(\text{St})} &= \frac{1}{c_\xi} \left( \frac{1}{AR} n_i n_j + \frac{1}{BR} (\delta_{ij} - n_i n_j) \right) \\ &\quad \times \left[ -I_{jk} \dot{\omega}_k^{(0)} - \frac{A^I - B^I}{B^I} I_{jk} \varepsilon_{klm} \omega_l^{(0)} n_m n_p \omega_p^{(0)} \right] \\ \omega_i^{(\text{Re}_s)} &= -\frac{1}{c_\xi} \left( \frac{1}{AR} n_i n_j + \frac{1}{BR} (\delta_{ij} - n_i n_j) \right) \int_V dV \tilde{U}_{kj} f_k(\mathbf{u}').\end{aligned}\quad (33)$$

Eq. (28) together with Eqs. (30) and (33) yield the effective angular velocity under the effect of weak particle and fluid inertia. From the equation of motion (7) we define the effective vector field

$$\dot{n}_i = \varepsilon_{ijk} \omega_j n_k \equiv \dot{n}_i^{(0)} + \text{St} \dot{n}_i^{(\text{St})} + \text{Re}_s \dot{n}_i^{(\text{Re}_s)}.\quad (34)$$

This vector field describes the time evolution of  $\mathbf{n}$ . The first term is the Jeffery vector field (31). The two new terms represent the effects of particle inertia and fluid inertia. The terms due to particle inertia are straightforward to evaluate directly, but the volume integral in Eq. (33) is very tedious to evaluate. To make the calculation feasible we exploit the symmetries of the problem.

## F. Symmetries of the effective equation of motion

Both correction terms in Eq. (34) are quadratic in the ambient flow gradient tensor  $A_{ij}^\infty$ . In other words, they are on the form

$$\dot{n}_i = C_{ijklm}^{(1)} O_{jk}^\infty O_{lm}^\infty + C_{ijklm}^{(2)} O_{jk}^\infty S_{lm}^\infty + C_{ijklm}^{(3)} S_{jk}^\infty S_{lm}^\infty,\quad (35)$$

where the tensorial coefficients  $C_{ijklm}^{(i)}$  are composed of the remaining available tensor quantities:  $n_p$  and  $\delta_{pq}$  ( $\varepsilon_{ijk}$  is already used in  $O_{ij}^\infty$ ). We make an exhaustive enumeration of all possible combinations, and then use the symmetries listed in Table I to remove or combine items in the list. For example we start by letting

$$C_{ijklm}^{(1)} = \sum_P \left[ \eta_1^{(P)} n_{p_1} \delta_{p_2 p_3} \delta_{p_4 p_5} + \eta_2^{(P)} n_{p_1} n_{p_2} n_{p_3} \delta_{p_4 p_5} + \eta_3^{(P)} n_{p_1} n_{p_2} n_{p_3} n_{p_4} n_{p_5} \right]\quad (36)$$

where the sum is over all  $5! = 120$  permutations  $P$  of  $(i, j, k, l, m)$ , and  $\eta_i^{(P)}$  are unique coefficients for each term. We include only odd powers of  $n_i$  as any even terms would break the particle inversion symmetry. We then insert this enumeration into the first term of Eq. (35), and contract and apply the first three symmetries in Table I until we reach a list of unique candidate terms. In this case the only two unique terms turn out to be  $O_{ij} O_{jk} n_k$  and  $n_i n_j O_{jk} O_{kl} n_l$ . Finally, we use the fact that the equation of motion may not change the magnitude of the unit vector  $\mathbf{n}$ . This constraint forces the coefficients of the two unique terms to be the same magnitude but opposite sign. Upon renaming the coefficients  $\pm\alpha_1$  we get the first term in Eq. (37). The other terms are derived similarly by inserting (36) into the other terms in Eq. (35). The result contains only six independent terms:

$$\begin{aligned}\dot{n}_i &= \alpha_1 (\delta_{ij} - n_i n_j) O_{jk}^\infty O_{kl}^\infty n_l \\ &\quad + \alpha_2 (\delta_{ij} - n_i n_j) S_{jk}^\infty O_{kl}^\infty n_l \\ &\quad + \alpha_3 (\delta_{ij} - n_i n_j) O_{jk}^\infty S_{kl}^\infty n_l \\ &\quad + \alpha_4 (\delta_{ij} - n_i n_j) S_{jk}^\infty S_{kl}^\infty n_l \\ &\quad + \alpha_5 (n_p S_{pq}^\infty n_q) O_{ij}^\infty n_j \\ &\quad + \alpha_6 (n_p S_{pq}^\infty n_q) (\delta_{ij} - n_i n_j) S_{jk}^\infty n_k.\end{aligned}\quad (37)$$

Here the scalar functions  $\alpha_1, \dots, \alpha_6$  are linear in  $\text{St}$  and  $\text{Re}_s$ , and depend on the aspect ratio  $\lambda$  in a non-linear (and unknown) way. These coefficients are determined by evaluating the vector field in Eq. (34) for six independent directions of  $\mathbf{n}$  and solving the resulting system of linear equations for  $\alpha_1, \dots, \alpha_6$ .

TABLE I. Symmetries constraining the form of the effective equation of motion, Eq. (34).

|  |                                    |
|--|------------------------------------|
| $S_{ii}^\infty = 0$  | Incompressible flow                |
| $S_{ij}^\infty = S_{ji}^\infty$                                  | $\mathbf{S}^\infty$ symmetric      |
| $O_{ij}^\infty = -O_{ji}^\infty$                                 | $\mathbf{O}^\infty$ anti-symmetric |
| $n_i \dot{n}_i = 0$  | Dynamics preserves magnitude       |
| $n_i \rightarrow -n_i \implies \dot{n}_i \rightarrow -\dot{n}_i$ | Particle inversion symmetry        |

In the particular case of a simple shear flow, we have explicitly (see Fig. 1 for the geometry)

$$O_{ij}^\infty = \frac{1}{2}(\delta_{i1}\delta_{j2} - \delta_{i2}\delta_{j1}), \quad S_{ij}^\infty = \frac{1}{2}(\delta_{i1}\delta_{j2} + \delta_{i2}\delta_{j1}). \quad (38)$$

We observe that for the simple shear  $O_{ij}^\infty O_{jk}^\infty = -S_{ij}^\infty S_{jk}^\infty$ , and  $S_{ij}^\infty O_{jk}^\infty = -O_{ij}^\infty S_{jk}^\infty$ . Then the form of the equation of motion simplifies to

$$\begin{aligned} \dot{n}_i = & \beta_1 (n_p S_{pq}^\infty n_q) (\delta_{ij} - n_i n_j) S_{jk}^\infty n_k \\ & + \beta_2 (n_p S_{pq}^\infty n_q) O_{ij}^\infty n_j \\ & + \beta_3 (\delta_{ij} - n_i n_j) O_{jk}^\infty S_{kl}^\infty n_l \\ & + \beta_4 (\delta_{ij} - n_i n_j) S_{jk}^\infty S_{kl}^\infty n_l, \end{aligned} \quad (39)$$

with

$$\begin{aligned} \beta_1 &= \alpha_6, \\ \beta_2 &= \alpha_5, \\ \beta_3 &= \alpha_3 - \alpha_2, \\ \beta_4 &= \alpha_4 - \alpha_1. \end{aligned} \quad (40)$$

Thus, for the case of the simple shear flow it suffices to evaluate the effective vector field in Eq. (34), in particular the volume integral in Eq. (33), with four independent values of  $\mathbf{n}$  in order to solve for the unknown scalar coefficients  $\beta_1, \dots, \beta_4$ .

### G. Evaluation of the volume integral in Eq. (33)

The volume integral in Eq. (33) contains four distinct terms:  $\partial_t u'_i$ , represents unsteady fluid inertia, and the three terms  $u_j^\infty \partial_j u'_i + u'_j \partial_j u_i^\infty + u'_j \partial_j u'_i$  represent convective fluid inertia. We compute these four terms using the explicit Stokes-flow solutions (17). While the Stokes flow has no explicit time dependence, both particle direction  $\mathbf{n}$  and angular velocity  $\boldsymbol{\omega}$  do. Thus each occurrence of  $n_k$  and  $\omega_k$  has to be differentiated to compute the contribution due to unsteady fluid inertia. The differentiation and tensor contractions are implemented by a custom set of pattern matching rules in Mathematica<sup>®</sup>. The calculation is both long and error prone. We have therefore automated every possible step, including solving the Stokes-flow equations.

We demonstrate the remainder of the procedure by a small example. Consider the contribution in the  $\hat{\mathbf{e}}_3$ -direction of Eq. (33) due to unsteady fluid inertia:

$$-\delta_{i3} \frac{1}{c_\xi} \left( \frac{1}{AR} n_i n_j + \frac{1}{BR} (\delta_{ij} - n_i n_j) \right) \frac{\text{Re}_s}{\text{St}} \int_V dV \tilde{U}_{kj} \partial_t u'_k. \quad (41)$$

We first perform the time derivatives on (17) in the manner explained above. Then we insert the components of  $\mathbf{n}$ , and the explicit form of the shear flow (38). At this point we can explicitly perform the sum over all repeated indices. The result in this example consists of 858 terms, after collecting terms with same spatial dependence. The terms have a prefactor that stem from the Stokes-flow coefficients (see Appendix A),

and a spatial dependence coming from  $r_i$  and the spheroidal integrals  $J_m^n$  and  $K_m^n$  (see Appendix B). For  $\mathbf{n} = [1/2, \sqrt{3}/2, 0]$  a typical term looks like this:

$$\frac{1575\alpha^2 C^R (A^S - 3C^S) (2B^R + C^R) r^2 r_2^3 K_7^0 K_9^1}{16(B^R)^2 c_\xi}$$

We note that the only spatial dependence on the azimuthal angle around the symmetry axis of the body comes from factors  $r_i$ . We introduce a rotated coordinate system in which  $r_i = R_{ji} r'_j$ , such that  $r'_1$  is along the particle symmetry axis (see Appendix B). This change of basis enables integration of one spatial coordinate.

After this operation 260 terms still remain which we program Mathematica<sup>®</sup> to express in spheroidal coordinates (Appendix C) and integrate over the remaining two spatial coordinates.

As a consistency check we have also evaluated the volume integral numerically over all three spatial dimensions by converting to spheroidal coordinates and choosing a specific value of  $\lambda$ . For extreme values of  $\lambda$  the numerics are difficult, nevertheless they serve as a check for a wide range of aspect ratios (see markers in Fig. 2).

## IV. RESULTS

### A. Effective equation of motion

We parametrize the vector  $\mathbf{n}$  in a spherical coordinate system  $(\theta, \varphi)$  with  $\theta$  the polar angle and  $\varphi$  the azimuthal angle (Fig. 1):

$$n_1 = \sin \theta \cos \varphi \quad n_2 = \sin \theta \sin \varphi, \quad n_3 = \cos \theta.$$

In these coordinates Eq. (39) is expressed as

$$\dot{\varphi}(\theta, \varphi) = \frac{1}{2} (\Lambda \cos 2\varphi - 1) + \frac{1}{8} \beta_1 \sin^2 \theta \sin 4\varphi - \frac{1}{4} \sin 2\varphi (\beta_2 \sin^2 \theta + \beta_3), \quad (42a)$$

$$\dot{\theta}(\theta, \varphi) = \Lambda \sin \theta \cos \theta \sin \varphi \cos \varphi + \frac{1}{4} \sin \theta \cos \theta (\beta_1 \sin^2 \theta \sin^2 2\varphi + \beta_3 \cos 2\varphi + \beta_4). \quad (42b)$$

We compute the contributions to  $\beta_\alpha$  from three sources: particle inertia, unsteady fluid inertia and convective fluid inertia. Although the result is only valid for neutrally buoyant particles ( $\text{Re}_s = \text{St}$ ), it is interesting to consider the contributions separately:

$$\beta_\alpha = \text{St} \beta_\alpha^{(P)} + \text{Re}_s \beta_\alpha^{(U)} + \text{Re}_s \beta_\alpha^{(C)} \quad (43)$$

The contribution from particle inertia is straightforward to compute and can be expressed in closed form as

$$\begin{aligned} \beta_1^{(P)} &= \frac{2B^I (C^R)^2}{(B^R)^3 c_\xi}, \\ \beta_2^{(P)} &= -\frac{C^R (A^I - 2B^I)}{(B^R)^2 c_\xi}, \\ \beta_3^{(P)} &= \frac{A^I C^R}{(B^R)^2 c_\xi}, \\ \beta_4^{(P)} &= -\frac{(A^I - B^I) (B^R)^2 + B^I (C^R)^2}{(B^R)^3 c_\xi}. \end{aligned} \quad (44)$$

The coefficients on the r.h.s. of these equations are tabulated for both prolate and oblate spheroids in Table III in Appendix A. The coefficients in Eq. (44) are shown as dotted lines in Fig. 2.

The expressions for the contributions from fluid inertia are very lengthy and not particularly instructive. We therefore present the full result graphically as function of aspect ratio  $\lambda$  in Fig. 2. In addition we give the asymptotic behavior of all contributions to  $\beta_\alpha$  in Table II in three limiting cases: thin oblate particles

TABLE II. Asymptotic results for  $\beta_\alpha$ . Contributions from particle inertia, unsteady fluid inertia, and convective fluid inertia are shown separately. Factors of  $\text{Re}_s$  and  $\text{St}$  are omitted.

| Thin oblate particles ( $\lambda \rightarrow 0$ )       |  |                                  |  |  |
|---|--|----------------------------------|--|--|
|   | Total  | Unsteady                         | Convective   | Particle   |
| $\beta_1$   | $\frac{11}{30}$                                    | $\frac{1}{5}$                    | $\frac{1}{6}$  | 0  |
| $\beta_2$   | $\frac{1}{10}$                                     | $-\frac{1}{20}$                  | $\frac{3}{20}$   | 0  |
| $\beta_3$   | $-\frac{1}{5}$                                     | $-\frac{3}{20}$                  | $-\frac{1}{20}$  | 0  |
| $\beta_4$   | $-\frac{1}{3}$                                     | $-\frac{3}{20}$                  | $-\frac{11}{60}$                                       | 0  |
| Nearly spherical particles ( $ \epsilon  \ll 1$ )       |  |                                  |  |  |
|   | Total  | Unsteady                         | Convective   | Particle   |
| $\beta_1$   | $\frac{137\epsilon^2}{294}$                        | 0                                | $\frac{163\epsilon^2}{490}$                            | $\frac{2\epsilon^2}{15}$                         |
| $\beta_2$   | $\frac{2\epsilon}{21} + \frac{81\epsilon^2}{245}$  | $\frac{62\epsilon^2}{525}$       | $\frac{\epsilon}{35} + \frac{37\epsilon^2}{294}$       | $\frac{\epsilon}{15} + \frac{13\epsilon^2}{150}$ |
| $\beta_3$   | $-\frac{2\epsilon}{7} - \frac{229\epsilon^2}{735}$ | $-\frac{58\epsilon^2}{525}$      | $-\frac{37\epsilon}{105} - \frac{227\epsilon^2}{1470}$ | $\frac{\epsilon}{15} - \frac{7\epsilon^2}{150}$  |
| $\beta_4$   | $\frac{8\epsilon}{21} - \frac{103\epsilon^2}{735}$ | 0                                | $\frac{11\epsilon}{35} - \frac{229\epsilon^2}{2450}$   | $\frac{\epsilon}{15} - \frac{7\epsilon^2}{150}$  |
| Thin prolate particles ( $\lambda \rightarrow \infty$ ) |  |                                  |  |  |
|   | Total  | Unsteady                         | Convective   | Particle   |
| $\beta_1$   | $\frac{7}{30 \log 2\lambda - 45}$                  | $\frac{1}{8 \log 2\lambda - 12}$ | $\frac{13}{120 \log 2\lambda - 180}$                   | 0  |
| $\beta_2$   | $\frac{1}{10 \log 2\lambda - 15}$                  | $\frac{1}{8 \log 2\lambda - 12}$ | $\frac{1}{20 \log 2\lambda - 60}$                      | 0  |
| $\beta_3$   | 0  | 0                                | 0  | 0  |
| $\beta_4$   | 0  | 0                                | 0  | 0  |

( $\lambda \rightarrow 0$ ), thin prolate particles ( $\lambda \rightarrow \infty$ ), and nearly spherical particles. For nearly spherical particles we define a small parameter  $\epsilon$  as follows

$$\lambda = \frac{1}{1 - \epsilon} \quad \text{for prolate spheroids } (\epsilon > 0),$$

$$\lambda = 1 + \epsilon \quad \text{for oblate spheroids } (\epsilon < 0).$$

The asymptotic results for  $\lambda \rightarrow 0$ ,  $\lambda \rightarrow \infty$ , and for  $|\epsilon| \rightarrow 0$  are shown as red dashed lines in Fig. 2.

## B. Linear stability analysis at infinitesimal $\text{Re}_s$

The effective equations of motion (42) have two special polar angles  $\theta$  across which no orbit may pass, regardless of the values of  $\beta_\alpha$ . These angles are  $\theta = 0$  (the vorticity direction) and at  $\theta = \pi/2$  (the flow-shear plane). In the Jeffery dynamics ( $\text{Re}_s = \text{St} = 0$ ) the two orbits are called ‘log-rolling’ and ‘tumbling’, and they are both marginally stable, just like all other Jeffery orbits. When the  $\beta_\alpha$  are non-zero but infinitesimal, the log-rolling and tumbling Jeffery orbits still exist for any finite aspect ratio, but their stabilities change.

We quantify how particle and fluid inertia lift the degeneracy of the Jeffery orbits by computing the stability exponents  $\gamma$  for the log-rolling ( $\gamma_{\text{LR}}$ ) and tumbling ( $\gamma_{\text{T}}$ ) orbits. The stability exponent is the exponential growth rate over one period of the orbit:

$$\gamma = T_p^{-1} \lim_{\delta\theta_0 \rightarrow 0} \log |\delta\theta(T_p)/\delta\theta_0| = T_p^{-1} \int_0^{-2\pi} \frac{d\varphi}{\dot{\varphi}} \frac{\partial\dot{\theta}}{\partial\theta}, \quad (45)$$

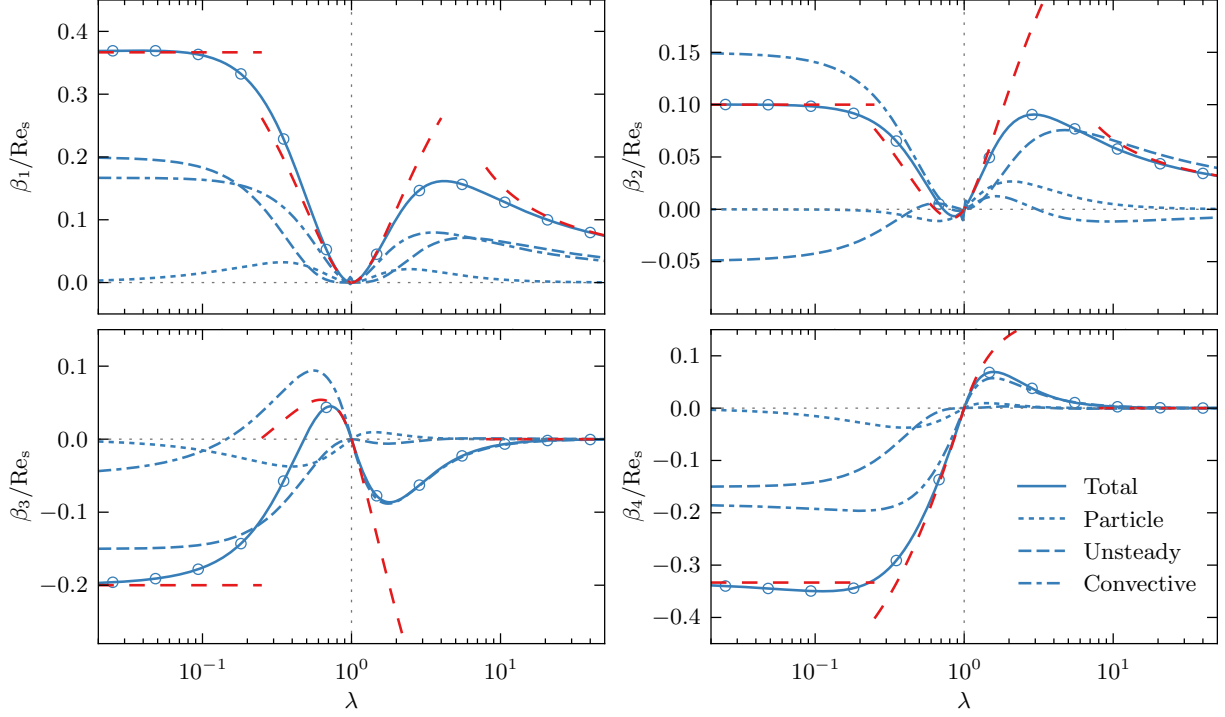


FIG. 2. *Color online.* Coefficients  $\beta_\alpha$  in Eq. (42),  $\alpha = 1.4$  as a function of particle aspect ratio  $\lambda$  for  $\text{Re}_s = \text{St}$ . Solid line shows the sum of all contributions. The other curves show the partial contributions from particle inertia (dotted), unsteady fluid inertia (dashed) and convective inertia (dash-dotted). The red dashed lines show the asymptotic solutions in Table II (first column). Circular markers show result of numerical integration of Eq. (33) for certain values of  $\lambda$ .

where  $T_p = 4\pi/\sqrt{1-\Lambda^2}$  is the Jeffery period. As  $\text{Re}_s \rightarrow 0$  we find

$$\gamma_T = -\frac{\beta_4}{4} + \frac{1-\sqrt{1-\Lambda^2}}{4\Lambda^2}(\Lambda\beta_2 - \beta_1), \quad \gamma_{\text{LR}} = \frac{\beta_4}{4}. \quad (46)$$

For  $\text{Re}_s = \text{St}$  these two exponents are shown as function of particle aspect ratio in Fig. 3. Also shown are their limiting behaviours in the thin oblate limit ( $\lambda \rightarrow 0$ )

$$\begin{aligned} \frac{\gamma_T}{\text{Re}_s} &\sim -\frac{1}{30} + \left(\frac{7}{30} - \frac{34}{45\pi} + \frac{7\pi}{80}\right)\lambda \\ &\quad + \frac{(-53248 + 19200\pi - 1728\pi^2 - 1728\pi^3 + 567\pi^4)\lambda^2}{8640\pi^2} \\ \frac{\gamma_{\text{LR}}}{\text{Re}_s} &\sim -\frac{1}{12} + \left(\frac{\pi}{80} - \frac{16}{45\pi}\right)\lambda + \left(\frac{5}{12} - \frac{256}{135\pi^2} + \frac{3\pi^2}{320}\right)\lambda^2, \end{aligned} \quad (47)$$

in the nearly spherical limit ( $\epsilon \rightarrow 0$ )

$$\frac{\gamma_T}{\text{Re}_s} \sim -\frac{2\epsilon}{21} - \frac{59\epsilon^2}{1680}, \quad \frac{\gamma_{\text{LR}}}{\text{Re}_s} \sim \frac{2\epsilon}{21} - \frac{103\epsilon^2}{2940}, \quad (48)$$

and in the thin prolate limit ( $\lambda \rightarrow \infty$ )

$$\frac{\gamma_T}{\text{Re}_s} \sim \frac{1}{45 - 30 \log 2\lambda}, \quad \frac{\gamma_{\text{LR}}}{\text{Re}_s} \sim \frac{1}{15\lambda^2}. \quad (49)$$

Fig. 3 shows that prolate spheroids of all aspect ratios are unstable at the log-rolling position, and stable at the tumbling orbit. For nearly spherical particles there is a bifurcation: log-rolling and tumbling switch stabilities. For oblate spheroids the log-rolling position is stable for any aspect ratio.

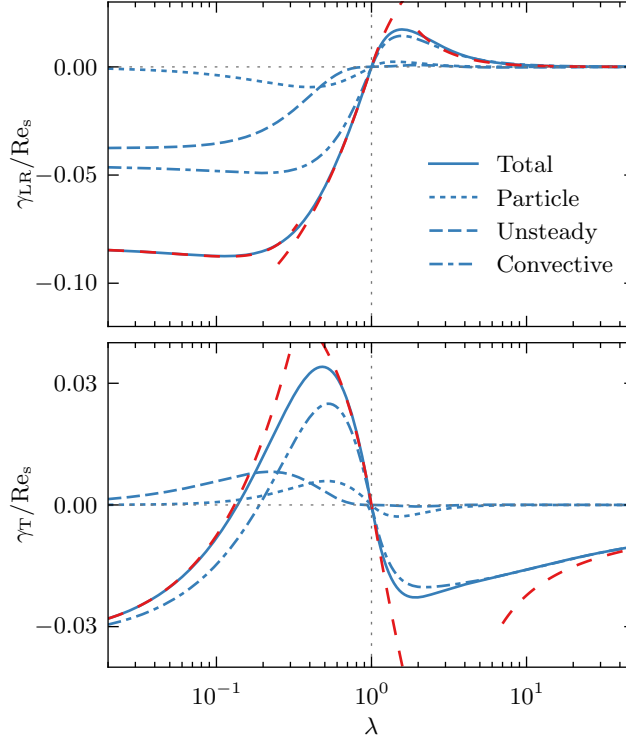


FIG. 3. *Color online.* Stability exponents of log-rolling (top panel) and tumbling (bottom panel) as a function of particle aspect ratio  $\lambda$  for infinitesimal  $\text{Re}_s = \text{St}$ . Solid line shows the sum of all contributions. The other curves show the partial contributions from particle inertia (dotted), unsteady fluid inertia (dashed) and convective inertia (dash-dotted). Red dashed lines show asymptotic results Eqns. (47-49).

For oblate particles there is a second bifurcation at  $\lambda_c \approx 1/7.3$  where the tumbling orbit becomes stable. Clearly, this behavior is caused by the convective inertia of the fluid (see the dash-dotted line in Fig. 3). For sufficiently oblate particles both log-rolling and tumbling orbits are stable, and the long-time dynamics depend on the initial orientation of the particle. Between the two now stable orbits a new unstable limit cycle is born, separating the two basins of attraction.

Fig. 4 shows how the shape of this limit cycle depends upon the particle aspect ratio. Close to the bifurcation the limit cycle lies in the neighbourhood of the tumbling orbit. But as  $\lambda \rightarrow 0$  the limit cycle approaches the log-rolling orbit. We have computed the stability exponent of the limit cycle at infinitesimal  $\text{Re}_s$  by numerically integrating Eqs. (42). The result is shown in Fig. 5. We see that  $\gamma_{LC} > 0$ , and its magnitude is of the same order as that of  $\gamma_T$ .

## V. DISCUSSION

*Effective equation of motion.* Eq. (42) is an effective equation of motion for the orientational dynamics of a neutrally buoyant spheroid in a simple shear flow. How the dynamics depends upon the particle aspect ratio is determined by four coefficients  $\beta_1, \dots, \beta_4$ . Fig. 2 shows the four functions  $\beta_\alpha(\lambda)$ . Limiting behaviours of the  $\beta_\alpha$  are tabulated in Table II. We see that the  $\beta$ -coefficients tend to zero as  $\lambda \rightarrow \infty$ , but they approach constants as  $\lambda \rightarrow 0$ . In both limits the contribution from particle inertia must tend to zero because the volume of the particle does. The effects of fluid inertia vanish as  $\lambda \rightarrow \infty$  because the particle effectively disappears in the slender-body limit, the perturbation caused by the particle decreases as  $\sim 1/\log \lambda$  as the asymptotic form in Table II shows. We remark that the leading-order term in this asymptotic form makes a substantial correction to the slender-body theory for aspect ratios of order 30.

An oblate particle, on the other hand, always presents no-slip boundaries to the fluid, with an area of the order of  $\sim a^2$  as  $\lambda \rightarrow 0$ . Therefore the contribution of fluid inertia approaches a constant. We note that the asymptotic forms of the coefficients  $\beta_\alpha$  listed in Table II yield accurate values for  $\lambda < 1/30$  and  $\lambda > 30$ , as

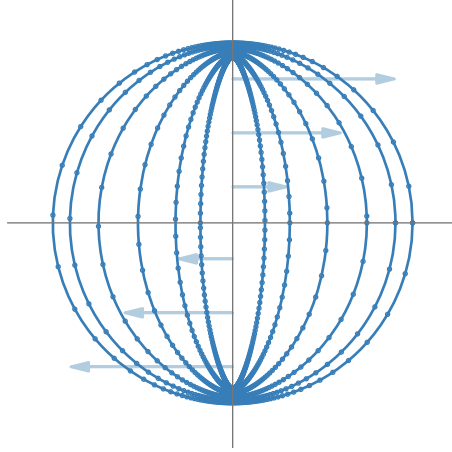


FIG. 4. *Color online.* The shape of the limit cycle for different aspect ratios  $\lambda < \lambda_c = 1/7.3$ . Trajectories are projected onto the unit disk by  $[X, Y] = \sqrt{1/(1-n_3)}[n_1, n_2]$  (equal area projection). The tumbling orbit is the unit circle, log-rolling is the center point. The flow-shear directions are indicated in the background. Parameters are, starting from the outermost (tumbling) orbit:  $\lambda = 1/7.2, 1/7.4, 1/8, 1/10, 1/15$  and  $1/25$ . Data created by numerically integrating Eq. (42) with  $\text{Re}_s = 10^{-2}$ . Markers are spaced equally in time.

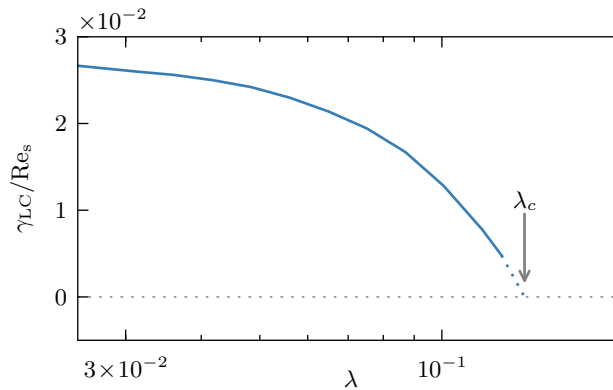


FIG. 5. *Color online.* Stability exponent  $\gamma_{LC}$  of the unstable limit cycle as a function of aspect ratio. Computed by numerically integrating Eqs. (42) for  $\text{Re}_s = 0.05$  (solid line). The limit cycle bifurcates at  $\lambda_c$ , indicated by an arrow and the dotted continuation of the numerical result.

Fig. 2 shows.

We see in Fig. 2 that the particle-inertia contribution to the coefficients  $\beta_\alpha$  is always much smaller than the fluid-inertia contributions. In general both unsteady and convective fluid inertia contribute, and it would be qualitatively wrong to neglect one of these terms. This is due to the fact that the timescale of the particle motion is the same as the timescale of the flow, and it raises the question under which circumstances both effects may matter for the tumbling of small particles in unsteady flows, and in particular in turbulence.

*Linear stability analysis at infinitesimal  $\text{Re}_s$ .* The stability exponents of tumbling and log-rolling orbits are shown in Fig. 3. We find that the log-rolling orbit is unstable for prolate spheroids of any aspect ratio, tumbling is stable for prolate spheroids, and no other orbit exist at infinitesimal  $\text{Re}_s$ . For moderately oblate particles with aspect ratios  $\lambda > \lambda_c \approx 1/7.3$  the stabilities are reversed: log-rolling is stable, tumbling is unstable, and no other periodic orbits exist for infinitesimal  $\text{Re}_s$ . At  $\lambda = \lambda_c$  there is a bifurcation where an unstable periodic orbit is born close to the tumbling orbit, which in turn becomes stable. As  $\lambda$  becomes even smaller, the unstable orbit moves closer to the log-rolling orbit (Fig. 4). We remark that the asymptotic forms (47) and (49) of the stability exponents yield very accurate approximations for the log-rolling exponent, save for aspect ratios close to unity. For the tumbling exponent the asymptotes do not work equally well.

Our results are in agreement with results of recent DNS studies<sup>3-6,18</sup> determining the orientational dynamics of a neutrally buoyant spheroid in a simple shear flow. These studies are conducted for a number

of different aspect ratios with shear Reynolds numbers ranging from moderate to large. At the smallest values of  $Re_s$  accessible in the DNS no stable log-rolling is found for prolate spheroids of any aspect ratio. For oblate particles with aspect ratio  $\lambda = 1/5$  DNS show stable log-rolling and unstable tumbling at the smallest  $Re_s$  that were simulated<sup>6</sup>, also in agreement with our results. There are no simulations for particles for  $\lambda < \lambda_c$  at small  $Re_s$ .

Saffman<sup>7</sup> predicted that log-rolling is stable for nearly spherical prolate particles, at variance with the behaviour described above. We do not know why the original calculation fails to give the correct stability of log-rolling. Since no details of the calculation are given it is difficult to figure out the precise origin of this discrepancy. Subramanian & Koch<sup>17</sup> also computed the stability of the log-rolling orbit for nearly spherical particles and came to the same conclusion as Saffman, different from ours. We have compared the small- $\epsilon$  limit of our calculation to the results of Ref. 17 and find that the particle-inertia correction to the equation of motion agrees, Eqs. (3.15) and (3.16) in Ref. 17. But the fluid-inertia correction does not satisfy the symmetries of the problem. We believe that this explains the discrepancy.

We have independently calculated the stability of log-rolling for nearly spherical particles by expanding the particle-angular velocity jointly in  $\epsilon$  and  $Re_s$ , using spherical harmonics as a basis set<sup>22</sup>. The results of this calculation agree to order  $\epsilon$  with the results presented above. Further we have checked that the particle-inertia correction in Eq. (42) is consistent with the results obtained in Ref. 9. We also compared the slender-body limit of our results to the prediction of Subramanian & Koch for the dynamics of slender fibres<sup>2</sup> and found that the fluid-inertia corrections agree (up to a factor of  $8\pi$ ).

These observations indicate that the results presented in this paper are correct, explain the results of DNS and resolve the puzzle concerning the stability of log-rolling of spheroids in a simple shear at small  $Re_s$ .

*A new benchmark for DNS at small  $Re_s$ .* Recently a number of groups have developed DNS codes based on the lattice Boltzmann method to simulate the dynamics of particles in flows<sup>3-6</sup>. Much effort is spent on validating the model, studying for instance the effects changing grid size, time step, size of the simulation box, and so forth. The benchmark adopted is often the question whether Jeffery orbits are seen for a neutrally buoyant spheroid in a simple shear at small Reynolds numbers. But the limit  $Re_s = 0$  can never be strictly reached in the simulations. DNS at small values of  $Re_s$  (specifically: in the linear regime), by contrast, allow precise comparisons with the results obtained in this paper. One could for instance compare trajectories, stability exponents, and period times. We thus expect that our results can serve as benchmarks for present and future DNS codes.

## VI. CONCLUSIONS

In this paper we have derived an effective equation of motion for the orientational dynamics of a neutrally buoyant spheroid suspended in a simple shear flow. The equation is valid for arbitrary aspect ratios and to linear order in  $Re_s$ , at small but finite shear Reynolds numbers. The effective equation of motion allows us to determine how the degeneracy of the Jeffery orbits is lifted by weak inertial effects. We have determined the bifurcations that occur at infinitesimal  $Re_s$  as the particle aspect ratio changes. For prolate spheroids log-rolling is unstable, for oblate spheroids it is stable. Tumbling in the shear plane is stable for prolate particles and unstable for nearly spherical oblate particles. For thin disks with aspect ratios  $\lambda < 1/7.3$ , both log-rolling and tumbling are stable. An unstable limit cycle separates the basins of attraction of the periodic orbits.

Our results imply that tumbling and log-rolling orbits survive a finite perturbation whose magnitude depends on the aspect ratio  $\lambda$ . It would be of interest to derive a bifurcation diagram in the  $\lambda$ - $Re_s$ -plane for small  $Re_s$ . We plan to determine how the small- $Re_s$  region of this diagram connects to the intricate bifurcation patterns that were found by Rosén, Lundell & Aidun<sup>5</sup> at larger shear Reynolds numbers. We expect that the results summarised here can guide numerical computations with the lattice Boltzmann method that become difficult at small  $Re_s$  and large aspect ratios.

<sup>1</sup>G. B. Jeffery, "The motion of ellipsoidal particles immersed in a viscous fluid," Proceedings of the Royal Society of London. Series A **102**, 161–179 (1922).

<sup>2</sup>G. Subramanian and D. L. Koch, "Inertial effects on fibre motion in simple shear flow," Journal of Fluid Mechanics **535**, 383–414 (2005).

<sup>3</sup>D. Qi and L. Luo, "Rotational and orientational behaviour of three-dimensional spheroidal particles in Couette flows," J. Fluid Mech. **477**, 201 (2003).

<sup>4</sup>H. Huang, X. Yang, M. Krafczyk, and X.-Y. Lu, "Rotation of spheroidal particles in Couette flows," J. Fluid Mech. **692**, 369–394 (2012).

<sup>5</sup>T. Rosén, F. Lundell, and C. K. Aidun, "Effect of fluid inertia on the dynamics and scaling of neutrally buoyant particles in shear flow," J. Fluid Mech. **738**, 563–590 (2014).

- <sup>6</sup>W. Mao and W. Alexeev, “Motion of spheroid particles in shear flow with inertia,” *J. Fluid Mech.* **749**, 145 (2014).
- <sup>7</sup>P. G. Saffman, “On the motion of small spheroidal particles in a viscous liquid,” *J. Fluid Mech.* **1**, 540 (1956).
- <sup>8</sup>F. Lundell and A. Carlsson, “Heavy ellipsoids in creeping shear flow: Transitions of the particle rotation rate and orbit shape,” *Physical Review E* **81**, 016323 (2010).
- <sup>9</sup>J. Einarsson, J. R. Angilella, and B. Mehlig, “Orientational dynamics of weakly inertial axisymmetric particles in steady viscous flows,” *Physica D: Nonlinear Phenomena* **278–279**, 79–85 (2014).
- <sup>10</sup>S. Kim and S. J. Karrila, *Microhydrodynamics: principles and selected applications*, Butterworth-Heinemann series in chemical engineering (Butterworth-Heinemann, Boston, 1991).
- <sup>11</sup>J. Einarsson, F. Candelier, F. Lundell, J. Angilella, and B. Mehlig, “The effect of weak inertia upon Jeffery orbits,” preprint (2015).
- <sup>12</sup>E. Y. Harper and I.-D. Chang, “Maximum dissipation resulting from lift in a slow viscous shear flow,” *J. Fluid Mech.* **33**, 209–225 (1968).
- <sup>13</sup>P. G. Saffman, “The lift on a small sphere in a slow shear flow,” *J. Fluid Mech.* **22**, 385–400 (1965).
- <sup>14</sup>E. J. Hinch and L. G. Leal, “The effect of Brownian motion on the rheological properties of a suspension of non-spherical particles,” *J. Fluid Mech.* **52**, 683–712 (1972).
- <sup>15</sup>C. J. Petrie, “The rheology of fibre suspensions,” *J. Non-Newton. Fluid* **87**, 369 – 402 (1999).
- <sup>16</sup>F. Lundell, D. Soderberg, and H. Alfredsson, “Fluid mechanics of papermaking,” *Annu. Rev. Fluid Mech.* **43**, 195–217 (2011).
- <sup>17</sup>G. Subramanian and D. L. Koch, “Inertial effects on the orientation of nearly spherical particles in simple shear flow,” *Journal of Fluid Mechanics* **557**, 257–296 (2006).
- <sup>18</sup>Z. Yu, N. Phan-Thien, and R. Tanner, “Rotation of a spheroid in a Couette flow at moderate Reynolds numbers,” *Phys. Rev. E* **76**, 026310 (2007).
- <sup>19</sup>H. Lorentz, “The theorem of Poynting concerning the energy in the electromagnetic field and two general propositions concerning the propagation of light,” *Versl. Kon. Akad. Wetensch. Amsterdam* **4**, 176 (1896).
- <sup>20</sup>J. Happel and H. Brenner, *Low Reynolds number hydrodynamics* (Kluwer Acad. Publisher, 1983).
- <sup>21</sup>A. T. Chwang and T. Y.-T. Wu, “Hydromechanics of low-Reynolds-number flow. Part 2. Singularity method for Stokes flows,” *Journal of Fluid Mechanics* **67**, 787–815 (1975).
- <sup>22</sup>F. Candelier, J. Einarsson, F. Lundell, B. Mehlig, and J. Angilella, “The role of inertia for the rotation of a nearly spherical particle in a general linear flow,” preprint (2015).

## Appendix A: Solutions to Stokes' equation

In this Appendix we solve the steady Stokes' equation for an arbitrarily aligned spheroid in a general linear flow  $\mathbf{u}^\infty = \mathbf{A}^\infty \mathbf{r}$ . The calculation is a special case of the calculation by Jeffery<sup>1</sup>. However, instead of the ellipsoidal harmonics that Jeffery used, we employ a finite multipole expansion, following Chwang and Wu<sup>21</sup>. The purpose of this Appendix is to derive an explicit closed form expression for the Stokes flow field, suitable for evaluation in the reciprocal theorem. For a more general description of the method we refer to the book by Kim and Karrila<sup>10</sup>.

*Formulation of the problem.* Stokes' equation reads:

$$\partial_j \partial_j u_i = \partial_i p, \quad \partial_i u_i = 0, \quad (\text{A1})$$

with no-slip boundary conditions on the surface  $S$  of the particle

$$u_i = \varepsilon_{ijk} \omega_j r_k \quad \text{for } \mathbf{r} \in S. \quad (\text{A2})$$

Here  $\omega_j$  is the angular velocity of the particle. Furthermore it is assumed that the flow remains unperturbed at infinitely far away from the particle

$$u_i = u_i^\infty \quad \text{as } |\mathbf{r}| \rightarrow \infty. \quad (\text{A3})$$

We solve for the disturbance flow  $u'_i = u_i - u_i^\infty$  that satisfies Stokes' equation (A1) with boundary conditions

$$u'_i = \varepsilon_{ijk} \omega_j r_k - u_i^\infty \quad \text{for } \mathbf{r} \in S, \quad u'_i = 0 \quad \text{as } |\mathbf{r}| \rightarrow \infty. \quad (\text{A4})$$

We decompose the linear background flow  $u_i^\infty$  into its symmetric and antisymmetric parts, defining the vector  $\Omega_i^\infty$  and strain  $S_{ij}^\infty$  by

$$u_i^\infty = A_{ij}^\infty r_j = \varepsilon_{ijk} \Omega_j^\infty r_k + S_{ij}^\infty r_j. \quad (\text{A5})$$

Finally, in terms of the 'slip angular velocity'  $\Omega_i = \Omega_i^\infty - \omega_i$ , the problem to be solved reads

$$\begin{aligned} \partial_j \partial_j u'_i &= \partial_i p', \quad \partial_i u'_i = 0, \\ u'_i &= -\varepsilon_{ijk} \Omega_j r_k - S_{ij}^\infty r_j \quad \text{for } \mathbf{r} \in S, \\ u'_i &= 0 \quad \text{as } |\mathbf{r}| \rightarrow \infty. \end{aligned} \quad (\text{A6})$$

*Multipoles.* We solve Eq. (A6) by a finite multipole expansion<sup>10,21</sup>. The multipoles are the Green's function for the Stokes' equation, and its derivatives. In this Appendix we use the shorthand notation  $\mathcal{G}_{ij,k} \equiv \partial_k \mathcal{G}_{ij}$ . The multipoles needed to solve for the fluid velocity field around particles in a linear flow are

$$\begin{aligned} \mathcal{G}_{ij} &= \frac{\delta_{ij}}{r} + \frac{x_i x_j}{r^3}, \\ \mathcal{G}_{ij,k} &= -\frac{\delta_{ij} x_k}{r^3} + \frac{\delta_{ik} x_j}{r^3} + \frac{\delta_{jk} x_i}{r^3} - \frac{3x_i x_j x_k}{r^5}, \\ \mathcal{G}_{ij,ll} &= \nabla^2 \mathcal{G}_{ij} = \frac{2\delta_{ij}}{r^3} - \frac{6x_i x_j}{r^5}, \\ \mathcal{G}_{ij,llk} &= \nabla^2 \mathcal{G}_{ij,k} = -\frac{6}{r^5} (\delta_{ij} x_k + \delta_{jk} x_i + \delta_{ik} x_j) + \frac{30x_i x_j x_k}{r^7}. \end{aligned} \quad (\text{A7})$$

The following two higher-order multipoles are required in the reciprocal theorem. We include them for reference:

$$\begin{aligned}
\mathcal{G}_{ij,km} &= \frac{\delta_{im}\delta_{jk}}{r^3} + \frac{\delta_{ik}\delta_{jm}}{r^3} - \frac{\delta_{ij}\delta_{km}}{r^3} - \frac{3x_i x_j \delta_{km}}{r^5} \\
&\quad - \frac{3x_j x_k \delta_{im}}{r^5} - \frac{3x_j x_m \delta_{ik}}{r^5} + \frac{3x_k x_m \delta_{ij}}{r^5} \\
&\quad - \frac{3x_i x_k \delta_{jm}}{r^5} - \frac{3x_i x_m \delta_{jk}}{r^5} + \frac{15x_i x_j x_k x_m}{r^7}, \\
\mathcal{G}_{ij,llkm} &= \frac{30x_i x_m \delta_{jk}}{r^7} + \frac{30x_i x_j \delta_{km}}{r^7} + \frac{30x_i x_k \delta_{jm}}{r^7} \\
&\quad + \frac{30x_j x_k \delta_{im}}{r^7} + \frac{30x_j x_m \delta_{ik}}{r^7} + \frac{30x_k x_m \delta_{ij}}{r^7} \\
&\quad - \frac{6\delta_{im}\delta_{jk}}{r^5} - \frac{6\delta_{ik}\delta_{jm}}{r^5} - \frac{6\delta_{ij}\delta_{km}}{r^5} \\
&\quad - \frac{210x_i x_j x_k x_m}{r^9}. \tag{A8}
\end{aligned}$$

Note that we use the ‘‘Oseen tensor’’ notation. The Green’s function for the Stokes’ equation is in fact  $G_{ij} = \mathcal{G}_{ij}/8\pi$ . It is convenient to split the dipole contribution  $\mathcal{G}_{ij,k}$  into its antisymmetric (‘rotlet’) and symmetric (‘stresslet’) parts. They are

$$\begin{aligned}
\mathcal{G}_{ij,k}^R &= \frac{1}{2} (\mathcal{G}_{ij,k} - \mathcal{G}_{ik,j}) = \frac{1}{r^3} (\delta_{ik}x_j - \delta_{ij}x_k), \\
\mathcal{G}_{ij,k}^S &= \frac{1}{2} (\mathcal{G}_{ij,k} + \mathcal{G}_{ik,j}) = \frac{\delta_{kj}x_i}{r^3} - \frac{3x_i x_j x_k}{r^5}. \tag{A9}
\end{aligned}$$

*Spheroidal multipoles.* Whereas the flow around a spherical particle may be represented by multipoles anchored at a single point, representing the flow around a spheroidal particle requires a weighted line distribution of multipoles<sup>10,21</sup>. We therefore define the ‘spheroidal multipoles’ as the following distributions, note especially the different weights for higher-order multipoles:

$$\begin{aligned}
\mathcal{Q}_{ij,k}^R(\mathbf{r}, \mathbf{n}) &= \int_{-c}^c d\xi (c^2 - \xi^2) \mathcal{G}_{ij,k}^R(\mathbf{r} - \xi \mathbf{n}), \\
\mathcal{Q}_{ij,k}^S(\mathbf{r}, \mathbf{n}) &= \int_{-c}^c d\xi (c^2 - \xi^2) \mathcal{G}_{ij,k}^S(\mathbf{r} - \xi \mathbf{n}), \\
\mathcal{Q}_{ij,ll}^Q(\mathbf{r}, \mathbf{n}) &= \int_{-c}^c d\xi (c^2 - \xi^2)^2 \mathcal{G}_{ij,ll}(\mathbf{r} - \xi \mathbf{n}). \tag{A10}
\end{aligned}$$

The constant  $c$  is related to the spheroidal geometry. Prolate and oblate coordinates are obtained by rotating an ellipse around its major or minor axis. We call the distance between the foci of the underlying ellipse  $d$ , and then  $c = d/2$  for prolate coordinates, and  $c = id/2$  for oblate coordinates (see definition of coordinate systems in Appendix C.)

In order to write down explicit tensor expressions for the spheroidal multipoles we introduce the integrals  $I_m^n$ ,  $J_m^n$  and  $K_m^n$  by

$$\begin{aligned}
I_m^n &= \int_{-c}^c d\xi \frac{\xi^n}{|\mathbf{r} - \xi \mathbf{n}|^m}, \\
J_m^n &= c^2 I_m^n - I_m^{n+2}, \\
K_m^n &= c^2 J_m^n - J_m^{n+2} = c^4 I_m^n - 2c^2 I_m^{n+2} + I_m^{n+4}. \tag{A11}
\end{aligned}$$

The spatial variation of the functions  $I_m^n$  depends upon  $|\mathbf{r}|^2$  and  $\mathbf{r} \cdot \mathbf{n}$  only. Further properties and evaluation of the integrals are discussed in Appendix B. With  $J_m^n$  and  $K_m^n$  we express the spheroidal multipoles explicitly, for example the spheroidal rotlet:

$$\begin{aligned}
\mathcal{Q}_{ij,k}^R(\mathbf{r}, \mathbf{n}) &= \int_{-c}^c d\xi \frac{c^2 - \xi^2}{|\mathbf{r} - \xi \mathbf{n}|^3} [\delta_{ik}(r_j - \xi n_j) - \delta_{ij}(r_k - \xi n_k)] \\
&= (\delta_{ik}r_j - \delta_{ij}r_k) J_3^0 + (\delta_{ij}n_k - \delta_{ik}n_j) J_3^1.
\end{aligned}$$

The integrals  $I_m^n$  play the same part in spheroidal geometry as does  $1/r^m$  in spherical geometry. The spheroidal stresslet and quadrupole are given by

$$\begin{aligned} \mathcal{Q}_{ij,k}^S(\mathbf{r}, \mathbf{n}) &= \delta_{kj}x_i J_3^0 - \delta_{kj}n_i J_3^1 - 3r_i r_j r_k J_5^0 - \delta_{jk}n_i J_3^1 \\ &\quad + 3(n_i r_j r_k + n_j r_i r_k + n_k r_i r_j) J_5^1 \\ &\quad - 3(r_i n_j n_k + r_j n_i n_k + r_k n_i n_j) J_5^2 \\ &\quad + 3n_i n_j n_k J_5^3, \end{aligned} \quad (\text{A12})$$

$$\begin{aligned} \mathcal{Q}_{ij,llk}^Q(\mathbf{r}, \mathbf{n}) &= -6(\delta_{jk}r_i + \delta_{ik}r_j + \delta_{ij}r_k)K_5^0 + 30r_i r_j r_k K_7^0 \\ &\quad + 6(\delta_{jk}n_i + \delta_{ik}n_j + \delta_{ij}n_k)K_5^1 \\ &\quad - 30(r_i r_j n_k + r_i r_k n_j + r_j r_k n_i)K_7^1 \\ &\quad + 30(n_i n_j r_k + n_i n_k r_j + n_j n_k r_i)K_7^2 \\ &\quad - 30n_i n_j n_k K_7^3. \end{aligned} \quad (\text{A13})$$

*Solution by a finite multipole expansion.* The spheroidal multipoles are functions that satisfy Stokes' equation, and a suitable linear combination of them also satisfies the no-slip boundary condition on the surface of a spheroid with symmetry axis  $\mathbf{n}$ . The remaining problem is to determine the coefficients for this linear combination.

Following Kim and Karrila<sup>10</sup> we use the following ansatz for the disturbance flow field:

$$\begin{aligned} u'_i &= \mathcal{Q}_{ij,k}^R \varepsilon_{jkl} [(A^R n_l n_m + B^R (\delta_{lm} - n_l n_m)) \Omega_m + C^R \varepsilon_{lmn} n_m S_{no} n_o] \\ &\quad + (\mathcal{Q}_{ij,k}^S + \alpha \mathcal{Q}_{ij,llk}^Q) \\ &\quad \times [(A^S n_{jklm}^A + B^S n_{jklm}^B + C^S n_{jklm}^C) S_{lm}^\infty - C^R (\varepsilon_{jlm} n_k n_m + \varepsilon_{klm} n_j n_m) \Omega_l], \end{aligned} \quad (\text{A14})$$

where

$$\begin{aligned} n_{jklm}^A &= (n_j n_k - \frac{1}{3} \delta_{jk})(n_l n_m - \frac{1}{3} \delta_{lm}), \\ n_{jklm}^B &= n_j \delta_{kl} n_m + n_k \delta_{jl} n_m + n_j \delta_{km} n_l + n_k \delta_{jm} n_l - 4n_j n_k n_l n_m, \\ n_{jklm}^C &= -\delta_{jk} \delta_{lm} + \delta_{jl} \delta_{km} + \delta_{kl} \delta_{jm} \\ &\quad + \delta_{jk} n_l n_m + \delta_{lm} n_j n_k - n_j \delta_{kl} n_m - n_k \delta_{jl} n_m \\ &\quad - n_j \delta_{km} n_l - n_k \delta_{jm} n_l + n_j n_k n_l n_m. \end{aligned} \quad (\text{A15})$$

Given the ambient strain  $S_{ij}^\infty$ , and angular slip velocity  $\Omega_i = \Omega_i^f - \omega_i^p$  we must determine seven unknown scalars, which may depend upon the particle shape:  $A^R$ ,  $B^R$ ,  $C^R$ ,  $A^S$ ,  $B^S$ ,  $C^S$ , and  $\alpha$ . When the coefficients are known, Eq. (A14) is the sought Stokes solution.

In order to match the linear boundary condition Eq. (A4) we need the combinations of  $J_m^n$  and  $K_m^n$  in the ansatz to be constant on the particle surface, much like the scalar function  $1/r^m$  is in spherical geometry.

Upon examination, the functions  $J_3^0$  and  $K_5^0$  are constant on the spheroidal surface. Further, the functions  $J_3^1$  and  $K_5^1$  can be written as  $J_3^1 = n_j r_j J_3'^1$  and  $K_5^1 = n_j r_j K_5'^1$ , where  $J_3'^1$  and  $K_5'^1$  are constant on the spheroidal surface. The remaining spheroidal functions  $J_5^n$  and  $K_7^n$  which appear in the ansatz (A14) are more complicated. However, it turns out that they appear only in the combinations  $J_5^n - 10\alpha K_7^n$ . We therefore choose

$$\alpha = \frac{J_5^0}{10K_7^0} \Big|_{\text{surface}} = \frac{1}{8(\lambda^2 - 1)}. \quad (\text{A16})$$

With this choice of  $\alpha$  it holds that, on the surface of the spheroid,

$$\begin{aligned} J_5^0 - 10\alpha K_7^0 &= 0, \\ J_5^1 - 10\alpha K_7^1 &= 0, \\ J_5^2 - 10\alpha K_7^2 &= \frac{1}{3} J_3'^1 - 2\alpha K_5'^1, \\ J_5^3 - 10\alpha K_7^3 &= \frac{5}{3} J_3^1 - \frac{42}{3} \alpha K_5^1, \end{aligned} \quad (\text{A17})$$

both for prolate and oblate spheroids.

In order to extract the six independent equations for the six remaining coefficients we exploit that the boundary condition must be satisfied for any choice of  $n_j$ ,  $\Omega_j$  and  $S_{jk}^\infty$ . First, with  $S_{jk}^\infty = 0$  we contract Eq. (A4) with  $n_i$ ,  $\varepsilon_{ijk}n_j\Omega_k$  and  $\varepsilon_{ipq}n_q\varepsilon_{pjk}n_j\Omega_k$ . Secondly, with  $\Omega_j = 0$ , we contract Eq. (A4) with  $n_i$ ,  $S_{ij}^\infty n_j$  and finally  $\varepsilon_{ijk}n_j S_{kl}^\infty n_l$ . These six equations together have only one solution. We tabulate the resulting expressions for both oblate and prolate spheroids in Table III.

Computing the torque on a body due to this flow is straightforward, because by construction<sup>21</sup> the torque on a body due to the rotlet flow  $u_i = \mathcal{G}_{ij,k}^R \varepsilon_{jkl} A_l$  is  $T_l^R = -16\pi A_l$ , where  $A_l$  is the rotlet strength. The minus sign is due to the fact that the torque is exerted on body by the flow. To compute the torque from the spheroidal rotlet (A10) we linearly superpose the contributions from all the contained rotlets. The torque from the flow  $u_i = \mathcal{Q}_{ij,k}^R \varepsilon_{jkl} B_l$  is therefore

$$T_l = -16\pi \int_{-c}^c d\xi (c^2 - \xi^2) B_l - \frac{64\pi c^3}{3} B_l \equiv c_\xi B_l. \quad (\text{A18})$$

The factor  $c_\xi$  depends only on the aspect ratio of the particle (see Table III).

## Appendix B: Spheroidal integrals

In order to solve Stokes' equation and evaluating the volume integrals in the reciprocal theorem we need to solve integrals on the form

$$I_m^n(|\mathbf{r}|^2, \mathbf{r} \cdot \mathbf{n}) = \int_{-c}^c d\xi \frac{\xi^n}{|\mathbf{r} - \xi \mathbf{n}|^m}. \quad (\text{B1})$$

First, when matching boundary conditions we must evaluate the integrals with  $\mathbf{r}$  on the surface of the spheroidal particle. Second, when evaluating the reciprocal theorem we need to integrate products of two or three  $I_m^n$  multiplied with the components of the spatial coordinate  $\mathbf{r}$  over the entire fluid volume outside the particle. Therefore we express the functions  $I_m^n$  in a spheroidal coordinate system with symmetry axis  $\hat{\mathbf{x}}'$  along  $\mathbf{n}$ . This is accomplished by a rotational change of variables  $\mathbf{r}' = \mathbf{R}\mathbf{r}$ ,  $\hat{\mathbf{x}}' = \mathbf{R}\mathbf{n}$ , where the latter equality defines a rotation  $\mathbf{R}$ . The absolute value (distance) between  $\mathbf{r}$  and  $\xi \mathbf{n}$  is preserved by a rotation, and the integral is transformed into

$$I_m^n = \int_{-c}^c d\xi \frac{\xi^n}{[(x' - \xi)^2 + (y')^2 + (z')^2]^{\frac{m}{2}}}. \quad (\text{B2})$$

This form is equivalent to the integrals  $B_{m,n}$  in Chwang and Wu<sup>21</sup>. Geometrically, Eq. (B1) represents a line source along the direction  $\mathbf{n}$ . The rotation  $\mathbf{R}$  places the line source along the  $x'$ -axis in an auxiliary coordinate system. The result is a function of  $|\mathbf{r}|^2$  and  $x' = \hat{\mathbf{x}}' \cdot \mathbf{r}' = \mathbf{n} \cdot \mathbf{r}$ .

Explicit expressions for  $I_m^n$  may be found by direct integration, or by a recursion formula<sup>21</sup>. Since we require only a finite number of integrals, we simply perform the direct integration once and for all and save the result in a table.

Finally, when evaluating the term corresponding to unsteady fluid inertia in the volume integral of the reciprocal theorem, we need to compute the derivatives of  $I_m^n$  with respect to the moving vector  $\mathbf{n}$ . By differentiating Eq. (B1) we derive the following formula:

$$\frac{\partial}{\partial n_i} I_m^n = m r_i I_{m+2}^{n+1} - m n_i I_{m+2}^{n+2}. \quad (\text{B3})$$

## Appendix C: Spheroidal coordinates

Both oblate and prolate spheroidal coordinates are extensions of a two-dimensional elliptic coordinate system  $(\xi_1, \xi_2)$ . The  $\xi_1$ -coordinate represents concentric ellipses, while  $\xi_2$  represents the corresponding hyperbolas. Their intersections give unique coordinates in the  $x$ - $y$ -plane. An azimuthal angle of revolution  $\phi$  denotes the extension into three dimensions.

*Oblate spheroidal coordinates.* Start with the  $x$ - $y$ -plane, and place an ellipse of focal distance  $d$  with its minor axis along the  $x$ -axis. Now revolve the ellipse by  $2\pi$  around the  $x$ -axis to produce an oblate spheroid.

Then  $\xi_1$  represents concentric oblate spheroidal surfaces,  $\xi_2$  represents the corresponding hyperbolic surfaces, and we call  $\phi$  the angle of revolution. The coordinate equations are

$$\begin{aligned} x &= \frac{d}{2} \xi_1 \xi_2, \\ y &= \frac{d}{2} \sqrt{\xi_1^2 + 1} \sqrt{1 - \xi_2^2} \cos \phi, \\ z &= \frac{d}{2} \sqrt{\xi_1^2 + 1} \sqrt{1 - \xi_2^2} \sin \phi. \end{aligned} \quad (\text{C1})$$

The coordinate ranges are  $0 \leq \xi_1 < \infty$ ,  $-1 \leq \xi_2 \leq 1$  and  $0 \leq \phi \leq 2\pi$ , and the volume element  $dV = \frac{1}{8} d^3 (\xi_1^2 + \xi_2^2) d\xi_1 d\xi_2 d\phi$ .

In this paper we treat oblate spheroids with dimensionless major axis length unity, and minor axis length  $\lambda$ . These lengths determine the focal distance  $d$  as

$$d = 2\sqrt{1 - \lambda^2}, \quad (\text{C2})$$

and the particle surface is parameterised by

$$\xi_1^{(p)} = \frac{\lambda}{\sqrt{1 - \lambda^2}}. \quad (\text{C3})$$

*Prolate spheroidal coordinates.* Start with the  $x$ - $y$ -plane, and place an ellipse of focal distance  $d$  with its major axis along the  $x$ -axis. Now revolve the ellipse by  $2\pi$  around the  $x$ -axis to produce a prolate spheroid. Then  $\xi_1$  represents concentric prolate spheroidal surfaces,  $\xi_2$  represents the corresponding hyperbolic surfaces, and we call  $\phi$  the angle of revolution. The coordinate equations are

$$\begin{aligned} x &= \frac{d}{2} \xi_1 \xi_2, \\ y &= \frac{d}{2} \sqrt{\xi_1^2 - 1} \sqrt{1 - \xi_2^2} \cos \phi, \\ z &= \frac{d}{2} \sqrt{\xi_1^2 - 1} \sqrt{1 - \xi_2^2} \sin \phi, \end{aligned} \quad (\text{C4})$$

The coordinate ranges are  $1 \leq \xi_1 < \infty$ ,  $-1 \leq \xi_2 \leq 1$  and  $0 \leq \phi \leq 2\pi$ , and the volume element  $dV = \frac{1}{8} d^3 (\xi_1^2 - \xi_2^2) d\xi_1 d\xi_2 d\phi$ .

In this paper we treat prolate spheroids with dimensionless major axis length unity, and minor axis length  $1/\lambda$ . These lengths determine the focal distance  $d$  as

$$d = 2 \frac{\sqrt{\lambda^2 - 1}}{\lambda}, \quad (\text{C5})$$

and the particle surface is parameterised by

$$\xi_1^{(p)} = \frac{\lambda}{\sqrt{\lambda^2 - 1}}. \quad (\text{C6})$$

TABLE III. Coefficients for Stokes-flow solutions and moments of inertia for prolate and oblate spheroids. These coefficients are collected in the book by Kim & Karrila<sup>10</sup>. We tabulate them here for convenience, and because our conventions differ slightly from those adopted in Ref. 10. We remark that some of the coefficients tabulated here assume imaginary values. All physical quantities come out to be real-valued.

---



---

| Expressions common to both prolate and oblate spheroids   |  |   |
|---|--|---|
| $\alpha = \frac{1}{8(\lambda^2-1)}$   | $A^R = \frac{\sqrt{\lambda^2-1}}{4(C-\lambda^3+\lambda)}$                | $B^R = \frac{\sqrt{\lambda^2-1}(\lambda^2+1)}{4(-2C\lambda^2+C+\lambda^3-\lambda)}$ |
| $C^R = \frac{(\lambda^2-1)^{3/2}}{4(-2C\lambda^2+C+\lambda^3-\lambda)}$   | $A^S = \frac{(\lambda^2-1)^{3/2}}{4(2C\lambda^2+C-3\lambda^3+3\lambda)}$ | $C^S = \frac{(\lambda^2-1)^{3/2}}{2(3C+2\lambda^5-7\lambda^3+5\lambda)}$            |
| $B^S = -\frac{(\lambda^2-1)^{3/2}(C\lambda+\lambda^4-3\lambda^2+2)}{8(-2C\lambda^2+C+\lambda^3-\lambda)(-3C\lambda+\lambda^4+\lambda^2-2)}$ |  |   |

---

| Expressions particular to prolate and oblate spheroids |  |  |
|--|--|--|
|  | Oblate ( $\lambda < 1$ )   | Prolate ( $\lambda > 1$ )  |
| $C$  | $-\sqrt{1-\lambda^2} \cot^{-1}\left(\frac{\lambda}{\sqrt{1-\lambda^2}}\right)$ | $\sqrt{\lambda^2-1} \coth^{-1}\left(\frac{\lambda}{\sqrt{\lambda^2-1}}\right)$ |
| $d$  | $2\sqrt{1-\lambda^2}$  | $\frac{2\sqrt{\lambda^2-1}}{\lambda}$  |
| $c$  | $\frac{id}{2}$   | $\frac{d}{2}$  |
| $c_\xi$  | $\frac{64}{3}i\pi(1-\lambda^2)^{3/2}$  | $-\frac{64\pi(\lambda^2-1)^{3/2}}{3\lambda^3}$                                 |
| $A^I$  | $\frac{8\pi\lambda}{15}$   | $\frac{8\pi}{15\lambda^4}$   |
| $B^I$  | $\frac{4\pi}{15}\lambda(\lambda^2+1)$  | $\frac{4\pi(\lambda^2+1)}{15\lambda^4}$  |

---



---